Constraint Release Effects in Monodisperse and Bidisperse Polystyrenes in Fast Transient Shearing Flows

Cattaleeya Pattamaprom* and Ronald G. Larson*

Department of Chemical Engineering, University of Michigan, Ann Arbor, Michigan 48109

Received January 22, 2001

ABSTRACT: Predictions of the Mead−Larson−Doi (MLD) and the Doi−Edwards−Marrucci−Grizzuti (DEMG) models[1] are compared with the rheological data in start up of steady shearing of concentrated bidisperse polystyrene solutions. Both the MLD and DEMG models are "tube" theories of flow with reptation, but the MLD theory includes both reptative and convective constraint-release effects, which are neglected in the DEMG theory. The adjustable parameters for the models are the reptation times ($\tau_{d,i}$) of each molecular weight component, and the plateau modulus (G_N^0). A procedure is given for obtaining the stretch times ($\tau_{s,i}$) from the reptation times. The convective constraint release included in the MLD model remedies the extreme shear thinning predicted by the DEMG model, and the reptative constraint release extends the good predictions found for monodisperse polymers to bidisperse systems, especially at steady state. In the transient start up of shear for monodisperse polymers, both models provide good predictions in both the viscosities and the first normal stress differences at low shear rates. At high shear rates, the MLD model, as well as the DEMG model, can predict the strain at the peak in stress accurately; however, the magnitude of the overshoots predicted by the MLD model are not as high as those of the DEMG model, with the latter predicting overshoots that are closer to the observed results.

I. Introduction

The seminal molecular theory of Doi and Edwards[2] for the rheological properties of entangled polymers is based upon the notion of reptation in a conceptual "tube" of constraints imposed by the mesh of surrounding polymer molecules. While this theory successfully predicts the rheological response of entangled polymers in step shear strains, it fails to provide accurate predictions in other nonlinear deformation histories including steady-state and start up of steady shear and extension. The drawbacks of the Doi−Edwards model were partially addressed by Marrucci and Grizzuti,[3] who combined stretching of the tube in fast flows with the Doi−Edwards reptation theory. This model, referred to as the DEMG (Doi−Edwards−Marruci−Grizzuti) model, was further extended by incorporating nonlinear segmental stretch into the model.[4−6] The DEMG model combines two major relaxation mechanisms: (1) retraction of the polymers in the stretched "tube," and (2) reptation of the linear polymer chain out of the tube. The DEMG model is able to predict the existence of normal-stress overshoots in start up of steady shearing, but otherwise does not significantly improve the predictions of the Doi−Edwards theory.[6−7]

Recently, the ideas of "convective constraint release" (CCR) of Marrucci (1996)[8] and Marruci and Ianniruberto (1997)[9] have been incorporated into the DEMG theory by Mead, Larson, and Doi (1998),[7] leading to a new model, the MLD (Mead−Larson−Doi) model, with greatly improved predictions of steady-state and transient rheological behavior of entangled polymers in shearing flows. The original MLD and DEMG models were developed for monodisperse polymers. For polydisperse polymers, it is well-known that reptative constraint release must be accounted for if even the linear viscoelastic properties are to be predicted. The simplest way to account for reptative constraint release is via the "double reptation" algorithm.[10−14] Since the MLD theory already contains the convective constraint release mechanism, addition of reptative constraint release can be accomplished easily by a straightforward extension of the MLD equations,[15] which we present below. Reptative constraint release could also easily be added to the DEMG equations. Nevertheless, in what follows, since we are interested in exposing the influence of both reptative and convective constraint release on the rheology of monodisperse and polydispserse polymers, we will leave out all forms of constraint release, including reptative constraint release, from the DEMG theory, while including both forms of constraint release in the MLD theory. The polydisperse DEMG theory that we present below is therefore a trivial extension of the monodisperse DEMG theory obtained by taking the stress to be a weight-average of the stresses obtained for each monodisperse component of the mixture. In comparing this form of the DEMG theory to experiments, we will point out which failings of this form of the DEMG theory arise from the absence of reptative constraint release, as opposed to absence of convective constraint release.

The numerical procedures required for calculating stress from the complete constitutive equations for both the DEMG and MLD models are considerably more complex than those of the original Doi−Edwards model, even for a single-component system. To investigate bidisperse or polydisperse polymers, a simplified version or "toy" version of the MLD model analogous to that proposed by Pearson et al. (1989)[1] for the DEMG model is preferable and will be utilized here. Note that the "toy" versions of the DEMG and MLD models account for only a single reptation time, and a single Rouse time for each polymer component (higher frequency contributions to the relaxation spectrum are neglected). They also assume that the orientation and stretching are both uniform along the polymer chain. Consequently, the primitive-path fluctuation mechanism is subsumed into reptation and thus indirectly accounted for by adjusting the disengagement time of the polymer. Hence, for well-

10.1021/ma010101x CCC: $20.00
Published on Web 06/21/2001

entangled polymer melts, the disengagement time (τ_d) is taken to be proportional to molecular weight to the power 3.4, rather than the power 3 in the original Doi–Edwards model.

In this paper, we analyze the "toy" version of the MLD and DEMG models for shearing flows of monodisperse and bidisperse polystyrenes in concentrated solutions for steady-state and transient start up of steady shearing flows. In both models, the nonlinear-spring elastic forces are accounted for by using the Pade′ approximation of the inverse Langevin function,[16] which is a simple, but more accurate, approximation than the better-known "Warner spring". The model parameters for both models are the plateau modulus (G_N^0), the fixed-tube disengagement time (τ_d), and the Rouse time (τ_s), the first two of which are fit to data for monodisperse solutions, and the third of which is obtained by a procedure described shortly.

II. Theoretical Background

II.1. Constitutive Equations. A. Simplified MLD Model. The constitutive equation of the "toy" MLD (Mead, Larson, and Doi) model[15] is as follows:

$$\frac{1}{\tau_{ij}} = \frac{1}{\lambda_i^2 \tau_{d,i}} + f(\lambda_i)\left(\kappa:\mathbf{S}_j - \frac{\dot{\lambda}_j}{\lambda_j} + \frac{1}{\lambda_j^2 \tau_{d,j}}\right) \quad (1)$$

$$\mathbf{S}_j = \sum_k w_k \int_{-\infty}^{t} \frac{dt'}{\tau_{jk}(t')} \exp\left[-\int_{t'}^{t} \frac{dt''}{\tau_{jk}(t'')}\right] \mathbf{Q}(\mathbf{E}(t,t')) \quad (2)$$

$$\dot{\lambda}_i = \lambda_i\, \kappa:\mathbf{S}_i - \frac{k_{s,i}(\lambda_i)}{\tau_{s,i}}(\lambda_i - 1) - \frac{1}{2}(\lambda_i - 1)\sum_j w_j\left(\kappa:\mathbf{S}_j - \frac{\dot{\lambda}_j}{\lambda_j} + \frac{1}{\lambda_j^2 \tau_{d,j}}\right) \quad (3)$$

$$\boldsymbol{\sigma} = 5G_N^0 \sum_i w_i k_{s,i}(\lambda_i)\lambda_i^2\, \mathbf{S}_i \quad (4)$$

Here $\boldsymbol{\sigma}$ is the stress tensor and G_N^0 is the plateau modulus. The subscripts i and j denote components of the molecular weight distribution having molecular weight M_i and M_j, respectively. w_i is the weight fraction of chain i, $\mathbf{S}_i$ is the orientation tensor, and κ is the deformation gradient tensor. λ_i, the stretch ratio, is the ratio of the current length, L_i, of a tube segment occupied by polymer chains of type i to the equilibrium tube segment length (L_{eq}). The switch function $f(\lambda_i) = 1/\lambda_i$ captures the transition of the constraint-release effect from tube orientation (eq 2) at low deformation rate to tube retraction (eq 3) at high deformation rate. $k_{s,i}(\lambda_i)$, the nonlinearity of the spring coefficient accounting for the finite extensibility of polymer chains, equals unity for linear springs and becomes much greater than unity as the spring becomes nearly fully stretched. $\tau_{d,i}$ is the fixed-tube disengagement time, and $\tau_{s,i}$ is longest Rouse time or "stretch time".

Note that in the limit of the linear viscoelastic regime, where λ_i remains unity, $\kappa:\mathbf{S}_j = \dot{\lambda}_j/\lambda_j = 0$, and $f(\lambda_i) = 1$, eq 1 reduces to the double-reptation formula

$$\frac{1}{\tau_{ij}} = \frac{1}{\tau_{d,i}} + \frac{1}{\tau_{d,j}}$$

where τ_{ij} is the average relaxation time for entanglements between chains i and j. Therefore, for monodisperse systems where $i = j$, the relaxation time ($\tau'_{d,i} \equiv \tau_{ii}$) equals $\tau_{d,i}/2$, where $\tau_{d,i}$ is the disengagement time for polymer i in a fixed tube with no constraint release. For chains with molecular weights less than the critical entanglement molecular weight M_c, the disengagement time $\tau'_{d,i}$ is set to be equal to $\tau_{s,i}$; that is, $\tau_{d,i} = 2\tau_{s,i}$.

Since the simplified model assumes uniform orientation and stretching along the polymer chain, the universal tensor, $\mathbf{Q}(\mathbf{E}(t,t'))$, is derived using the "independent alignment approximation"[2]

$$\mathbf{Q}(\mathbf{E}(t,t')) \equiv \left\langle \frac{\mathbf{E}(t,t')\cdot u'\mathbf{E}(t,t')\cdot u'}{|\mathbf{E}(t,t')\cdot u'|^2} \right\rangle_0$$

where $\mathbf{E}(t,t')$ is the deformation gradient history, u' is a unit vector distributed randomly over the unit sphere, and $\langle\ \rangle_o$ represents an ensemble average of all u' over an isotropic state.

Constraint release shows up in the last terms of eqs 1 and 3. Equation 1 describes the relaxation rate, which is a linear combination of the reptation rate and constraint-release rates. The first two terms in parentheses in eq 1 describe the convective constraint release (CCR); the last term is due to reptative constraint release. Equation 3 describes the stretch rate of the primitive path; the stretch rate is slowed by the same constraint-release term that appears in eq 1. CCR is believed to induce tube shortening when a polymer chain is highly stretched ($\lambda_i > 1$) and to induce tube reorientation at low stretch ratios ($\lambda_i \approx 1$). $f(\lambda_i)$ in eq 1, which equals $1/\lambda_i$, serves as a crossover function between the tube-shortening and the tube-reorientation effects of constraint release (Mead, Larson, and Doi, 1998).[7] In the limit of linear viscoelasticity, $\lambda_i = 1$, $\kappa:\mathbf{S} = 0$, and $\mathbf{Q} = {}^1/_5\gamma$, where γ is the linear–viscoelastic strain tensor. In this limit, all CCR terms vanish, and this set of equations collapses to the double reptation formalism with a single terminal relaxation time.

B. The DEMG Model (Pearson et al. 1989).[1] The constitutive equation for DEMG model is similar to the MLD model except without the reptative and convective constraint release terms (the last terms of eqs 1 and 3):

$$\mathbf{S}_i = \int_{-\infty}^{t} \frac{dt'}{\tau'_{d,i}} \exp\left[-\frac{(t-t')}{\tau'_{d,i}}\right] \mathbf{Q}(\mathbf{E}(t,t')) \quad (5)$$

$$\dot{\lambda}_i = \lambda_i\, \kappa:\mathbf{S}_i - \frac{k_{s,i}(\lambda_i)}{\tau_{s,i}}(\lambda_i - 1) \quad (6)$$

$$\boldsymbol{\sigma} = \sum \boldsymbol{\sigma}_i = 5G_N^0 \sum_i w_i k_{s,i}(\lambda)\lambda_i^2\, \mathbf{S}_i \quad (7)$$

The variables used here are consistent with the above MLD model. In the linear viscoelastic limit, the DEMG model reduces to the original reptation model of De Gennes (1971),[17] with only the slowest relaxation mode retained. As mentioned earlier, the original version of the DEMG model,[1,3] which was developed for monodisperse polymers, does not contain any form of constraint releases. The polydisperse DEMG theory that we present here is a trivial extension of the monodisperse DEMG theory obtained by taking the stress to be a weight-average of the stresses obtained for each monodisperse component of the mixture. Without the reptative-constraint-release terms, the relaxation time appearing in eq 5 is taken to be $\tau'_{d,i}$, which is related to the

characteristic disentanglement time $\tau_{d,i}$ in the MLD model by $\tau'_{d,i} = \tau_{ii} = \tau_{d,i}/2$.

II.2. Applications to Start Up of Shearing Flows. In this paper, we will explore the predictions made by the "toy" MLD and "toy" DEMG model for start up of shear and steady-state shear in monodisperse and binary mixtures of linear polymers. The adjustable parameters for both models are the fixed-tube disengagement time $\tau_{d,i}$, the plateau modulus G_N^0, and the "stretch time" $\tau_{s,i}$, the first two of which are obtained by fitting the model predictions with the monodisperse experimental data for each molecular weight component at steady-state and the third of which is obtained by a procedure described below. The numerical calculations for both models are obtained by finite difference approximation. The step sizes (Δt) used here are inversely proportional to the shear rates ($\dot\gamma$). The optimum step sizes were confirmed by comparing the results with those using smaller time steps. We found that, $\Delta t = 0.001/\dot\gamma$ usually provides accurate results. By applying the appropriate constitutive equations mentioned in section II.1, the shear viscosity (η), the first normal stress difference (N_1), the stretch ratio (λ_i), and the orientation tensor ($\mathbf{S}_i$) can be predicted. In a shearing flow, the variables used in eqs 1−7 are described below.

The velocity gradient tensor (κ), and the Finger tensor ($\mathbf{B} = \mathbf{E}^T\cdot\mathbf{E}$) can be written as

$$\kappa = (\nabla v)^{\mathrm{T}} = \begin{pmatrix} 0 & \dot\gamma & 0 \\ 0 & 0 & 0 \\ 0 & 0 & 0 \end{pmatrix} \mathbf{B} = \begin{pmatrix} 1+\gamma^2 & \gamma & 0 \\ \gamma & 1 & 0 \\ 0 & 0 & 1 \end{pmatrix}$$

where the shear strain, γ, is a function of the past time t' and the present time t. For a shearing flow that starts up at time 0 from a state of rest, γ is given by

$$\gamma = \begin{bmatrix} \dot\gamma(t-t'); & \text{for } t' > 0 \\ \dot\gamma t; & \text{for } t' > 0 \end{bmatrix}$$

The universal tensor $\mathbf{Q}$ is approximated using Curie's formula,[19] namely

$$\mathbf{Q} \approx \left(\frac{1}{J-1}\right)\mathbf{B} - \left(\frac{1}{(J-1)(I_2+13/4)^{1/2}}\right)\mathbf{C}$$

where $\mathbf{C}$ is the Cauchy tensor, defined by $\mathbf{C} = \mathbf{B}^{-1}$. I_1 is the trace of the tensor $\mathbf{B}$, and I_2 is the trace of the tensor $\mathbf{C}$. J is related to I_1 and I_2 by $J \equiv I_1 + 2(I_2+13/4)^{1/2}$.

The convection rate of the mesh of entanglements, $\kappa:\mathbf{S}$, is given by

$$\kappa:\mathbf{S} = \begin{pmatrix} 0 & \dot\gamma & 0 \\ 0 & 0 & 0 \\ 0 & 0 & 0 \end{pmatrix}; \begin{pmatrix} \mathbf{S}_{11} & \mathbf{S}_{12} & \mathbf{S}_{13} \\ \mathbf{S}_{21} & \mathbf{S}_{22} & \mathbf{S}_{23} \\ \mathbf{S}_{31} & \mathbf{S}_{32} & \mathbf{S}_{33} \end{pmatrix} = \dot\gamma \mathbf{S}_{12} \qquad (8)$$

The nonlinearity of the spring coefficient, k_s, is approximated by the normalized Pade′ inverse Langevin function[16] as $k_s = [(3-\alpha^2)/(1-\alpha^2)]/[(3-\beta^2)/(1-\beta^2)]$, where $\alpha = L_i/L_{max}$ and $\beta = L_{eq}/L_{max}$. L_{max}, the maximum length to which a tube segment can be stretched, is given by $L_{max} = 0.82\, l_0 N_e$, where l_0 is the backbone bond length (=1.54 Å for a carbon−carbon bond). N_e, the number of backbone bonds in an entanglement spacing, is calculated from $N_e = jM_e/M_o$, where the molecular weight between entanglements (M_e) of a polymer in solution is approximated using Ferry's definition, i.e., $M_e = \rho RT/G_N^0$ (further discussion on the choice of M_e for polymer solutions is given in section IV.1) M_o is the monomer molecular weight (equals 104 for polystyrene), and j is the number of the backbone bonds in a monomer ($j = 2$ for polystyrene). L_{eq}, the equilibrium length of a tube segment, equals $\sqrt{C_\infty N_e l_0^2}$, where C_∞ is the characteristic ratio. The value of C_∞ is normally in the range of 5−10, and is 9.6 for polystyrene.[18] The shear viscosity η and the viscosity contribution η_i from each polymer component are defined as

$$\eta = \frac{\sigma_{12}}{\dot\gamma} \quad \text{and} \quad \eta_i = \frac{\sigma_{12,i}}{\dot\gamma}, \quad \text{where } \boldsymbol{\sigma}_i = w_i(5G_N^0 k_{s,i}\lambda_i^2 \mathbf{S}_i)$$

III. Experimental Section

III.1. Materials and Methods. Highly entangled bidisperse polystyrene solutions were prepared at 7% volume fraction in the solvent tricresyl phosphate (TCP). This relatively low volume fraction of polymer leads to low normal stresses, thus delaying the onset of edge fracture to very high shear rates.[20] The delayed edge fracture allows us to measure stresses in start-up of shear over a wide range of shear rates. Both monodisperse and bidisperse high molecular-weight polystyrenes were prepared from the two monodisperse polystyrene samples obtained from Tosohaas Inc. The molecular weight of the longer-chain polymer is 8.42×10^6 ($M_w/M_n = 1.14$) and of the shorter-chain polymer is 2.89×10^6 ($M_w/M_n = 1.09$). The ratios of the long- to short-chain polymer volume fractions were chosen to be 0/100, 20/80, 40/60, 60/40, 80/20, and 100/0. The samples were prepared by dissolving weighed amounts of the individual polystyrene and TCP components in a large amount of cosolvent (dichloromethane). Most of the cosolvent evaporated out in the hood. The remaining cosolvent was completely removed by keeping the samples under vacuum until the weight of samples reduced to the expected weight without cosolvent (which took about 3 weeks). The molecular weights and polymer concentrations in each sample are shown in Table 1.

Table 1. Composition and Concentration of Polymer Solutions

sample no.	overall polymer vol fraction, %	ratio of 8.42M:2.89M
1	7	0/100
2	7	20/80
3	7	40/60
4	7	60/40
5	7	80/20
6	7	100/0

III.2. Rheological Measurements. The rheological properties of the polymer samples were measured on an ARES rheometer, a strain-controlled rheometer equipped with a force-rebalanced transducer from Rheometric Scientific Inc. The force-rebalanced transducer counteracts the normal force compliance and allows accurate measurements of the time-dependent first normal stress difference. Cone-and-plate fixtures were used with a cone angle of 0.1 rad and a radius of 1.25 cm.

Both dynamic oscillatory shearing and start-up of steady shearing were carried out at 40 °C. The dynamic oscillatory measurements were done over the frequency range 0.001 to 100 s^{-1}. The dynamic oscillatory viscosities $\eta^*(\omega)$ of the monodisperse and bidisperse solutions are shown in Figure 1. For the start up of shear measurements, the zero-shear viscosity increases from 4×10^3 to 1.8×10^5 P as the fraction of long chains (8.42 M) increases from zero to unity. The linear viscoelastic regime extends up to around 0.4 s^{-1} for pure 2.89 M and up to around 0.01 s^{-1} for pure 8.42 M, The range of shear rates was limited by the sensitivity and the maximum torque and normal force of the instrument (i.e., 0.2−2000 g cm. for torque, and 2−2000 g cm. for normal force.). The upper limit of the shear rate is also dependent on the visible appearance of edge fracture, which first occurred at progressively lower shear rate as the polymer became more viscous.

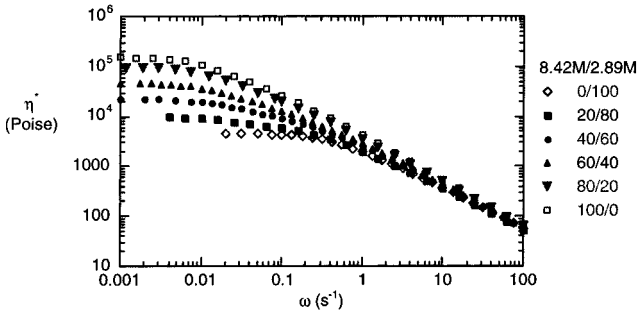

Figure 1. Dynamic oscillatory viscosities (η^*) for the binary-blend solutions of polystyrenes in Table 1.

The edge fracture started to become evident at long time after start up at moderate shear rates, where the appearance of the sample's meniscus was closely monitored, and the tests either reached steady state before the edge fracture began or were stopped at the onset of edge fracture. Any experimental data obtained after the appearance of edge fracture were discarded. To check repeatability, the rheological measurements were repeated at each shear rate for every sample both within the same batch of sample, and with a newly prepared sample.

For start up of shear, at low shear rate, both the shear stress and the first normal stress difference increase monotonically with time until attainment of steady state. At moderate shear rates, overshoots in shear stress start to appear; the overshoots in normal stress become noticeable as the shear rate is increased further. At still higher shear rates, we also observed undershoots in shear stress following the overshoots. The phenomenon of undershoots following stress overshoots has been observed earlier.[21−24] The reported relationships for instrument response times in torsion (λ_T) and in axial thrust (λ_A) indicates that the instrument response times are proportional to the zero-shear viscosity and the plate radius, and inversely proportional to the cone angle.[25,26] The larger the response times, the longer it takes for the measurements to reach reliable stress values. For the systems considered here, the compliance is irrelevant since λ_T and λ_A are very small (i.e., $\lambda_T = 0.002$ s and λ_A is negligible). The delays in the response time present at times shorter than about 0.1 s were due to the finite response time of the motor combined with the communication delay from the motor to the transducer.[27] The steady-state data were obtained from the start up of shear experiments after the stresses leveled off.

IV. Results and Discussion

Here we explain how we determined the MLD and DEMG model parameters, and compare the predictions of the models with our experimental data at steady state and during the transient start up of shear.

IV.1. Determination of the Model Parameters. The model parameters for both the MLD and DEMG models are the plateau modulus (G_N^0), the disengagement times ($\tau_{d,1}$ and $\tau_{d,2}$), and the longest Rouse times ($\tau_{s,1}$ and $\tau_{s,2}$) for the two components. We obtained G_N^0 and $\tau_{d,i}$ by fitting the steady-state predictions of the DEMG and MLD models to the experimental data for monodisperse polymer solutions of each molecular weight component i. The fits in the intermediate regime will provide the value of the plateau modulus G_N^0, whereas the ones in the low-shear-rate regime supply $\tau_{d,i}$. We calculated the Rouse "stretch" time $\tau_{s,i}$ for each component from the relationship[2] $\tau_{s,i} \propto M_i^2$ and our assumption that $\tau'_{d,i}$ and $\tau_{s,i}$ are equal at the critical entanglement molecular weight M_c (i.e., $\tau_{s,M_c} = \tau'_{d,M_c}$). Since the disengagement time (τ'_{d,M_c}) for a polymer with molecular weight M_c equals

$$\tau'_{d,i}\left(\frac{M_c}{M_i}\right)^{3.4} = \frac{1}{2}\tau_{d,i}\left(\frac{M_c}{M_i}\right)^{3.4}$$

we thereby obtain $\tau_{s,i}$ from the relation

$$\tau_{s,i} = \frac{1}{2}\tau_{d,i}\left(\frac{M_c}{M_i}\right)^{1.4}$$

Here, we assumed that M_e and M_c for the polystyrene solutions are inversely proportional to the volume fraction ϕ of polymers in the solution, i.e. $M_e = M_{e,melt}/\phi$ and $M_c = M_{c,melt}/\phi$, where the subscript "melt" represents the parameter for polymer melts. For polystyrene, $M_e = 16\,625$, and $M_c = 35\,000$ (Fetters et al., 1994).[18] This method of Rouse-time calculation leads to good fits of the MLD model with experimental data for all of the monodisperse samples and the binary blends, considered here. For the MLD model, the parameters obtained from the method mentioned above are $G_N^0 = 3000$ dyn/cm^2, the characteristic times $\tau_{d,1} = 3.06$ s, $\tau_{s,1} = 0.13$ s for sample 1 (the monodisperse solution with polystyrene molecular weight 2.89×10^6), and $\tau_{d,2} = 63.3$ s, $\tau_{s,2} = 0.6$ s for sample 6 (the monodisperse solution with weight 8.42×10^6). The best-fit value of G_N^0 mentioned above is not consistent with that obtained from the relationship between the plateau modulus in the melt state and in solutions. From Ferry's relationship between G_N^0 and M_e,[28] i.e., $G_N^0 = (\rho RT)/(M_e)$, where $\rho = \phi\rho_{melt}$ and ρ_{melt} is the density of solvent-free polystyrene melt, the plateau modulus of a 7% PS solution should have been $G_N^0 = (\phi^2\rho_{melt}RT)/(M_{e,melt}) = \phi^2 G_{N,melt}^0 = 10^4$ dyn/cm^2, where $G_{N,melt}^0 = 2 \times 10^6$ dyn/cm^2. This value of G_N^0 is three times higher than the best-fit value of G_N^0(3000 dyn/cm^2). This might indicate that the formulas ($M_e = (M_{e,melt})/(\phi)$ and ($M_c = (M_{c,melt})/(\phi)$ are not accurate for the solutions studied here. Nevertheless, we will find that the values of $\tau_{s,i}$ obtained from the procedure presented above give very good agreement with the steady shear data for monodisperse solutions, and so will be retained in what follows. The difference in G_N^0 could be related to a higher concentration dependence, i.e., $\phi^{2.3-2.4}$ as reported in the literature.[29,30] Note that we did not obtain the model parameters from fitting the double reptation scheme to the linear viscoelastic data. This is because the predictions of the double reptation model we used (with a single relaxation time) are not accurate beyond the low-frequency limit, thus making the appropriate value of G_N^0 difficult to justify from this comparison (Figure 2). As can be seen, the parameters that provide the best fits to the steady-shear data did not give a good prediction to the linear viscoelastic oscillatory data.

For the DEMG model, at low shear rates, the model collapses to the simple reptation model, instead of double reptation as in the MLD model; therefore, the parameter $\tau'_{d,i}$ used in the DEMG model is related to $\tau_{d,i}$ of the MLD model by $\tau'_{d,i} = \tau_{d,i}/2$. At high shear rates, the DEMG model predicts a highly oriented structure, causing the predictions of viscosities and first normal stress differences at high shear rates to be lower than those of the experimental data. One could try to compensate for the orientation of the chain by accelerating the stretching via increasing the Rouse time $\tau_{s,i}$, as shown in Figures 3 and 4 for the low-molecular-weight (sample 1) and the high-molecular-weight (sample 6) polystyrene solutions, respectively. As can be seen, even

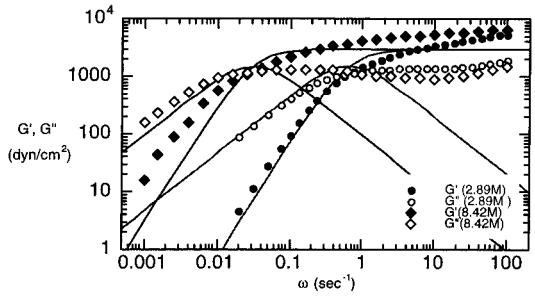

Figure 2. Comparison of the G' and G'' curves predicted by the double reptation model (with a single relaxation time) with experimental data for polystyrene solution sample 1(pure 2.89 M) and sample 6 (pure 8.42 M) at 40 °C. The symbols are the experimental data and the lines are the predictions using the double reptation model. The parameter values, G_N^0, and τ_d were obtained from fits to the steady-state viscosity and first normal stress differences.

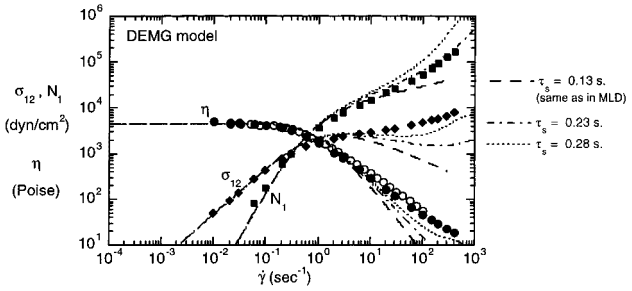

Figure 3. Comparison of the steady-state shear viscosity η and first normal stress difference N_1 predicted by the DEMG model with experimental data for polystyrene solution sample 1(pure 2.89 M) at 40 °C. The hollow circles are for the dynamic viscosity $\eta^*(\omega)$. The lines show the DEMG predictions using different values of the longest "Rouse" time $\tau_{s,}$. For this figure, we also show the shear stress $\sigma = \eta(\dot{\gamma})\dot{\gamma}$.

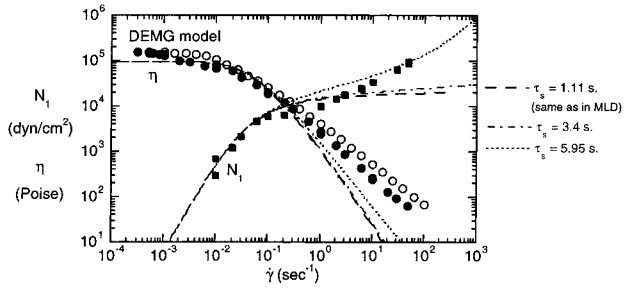

Figure 4. Same as Figure 3, except for sample 6 (pure 8.42 M). The shear stress is not shown here.

though the DEMG prediction for sample 1 can be improved by increasing the Rouse time $\tau_{s,i}$ (Figure 3), such adjustment could not capture accurately the shape of the experimental curves for sample 6, regardless of the value of $\tau_{s,2}$ (Figure 4). Since adjustment of the Rouse times did not consistently improve the prediction of the DEMG model, we decided to adopt the same values of $\tau_{s,i}$'s as those of the MLD model, i.e., $G_N^0 =$ 3000 dyn/cm^2, $\tau'_{d,1} = 1.53$ s, $\tau_{s,1} = 0.13$ s for sample 1, and $\tau'_{d,2} = 31.65$ s, $\tau_{s,2} = 0.6$ s for sample 6.

Comparisons of the model predictions and the experimental data using the above-mentioned model parameters will be shown in the following sections.

IV.2. Steady Shear Predictions of the Binary Blends. In what follows, the steady-state values of the experimental shear viscosities, shear stresses, and first normal stress differences as functions of shear rate are compared with the predictions of the "toy" versions of

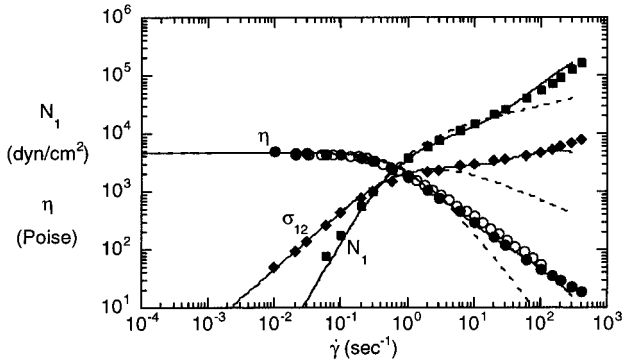

Figure 5. Comparison of the steady-state shear viscosity η and first normal stress difference N_1 predicted by the MLD (solid lines) and DEMG (broken lines) models with experimental data for polystyrene solution sample 1 (pure 2.89 M) at 40 °C. The model parameters are those specified in section IV. I.

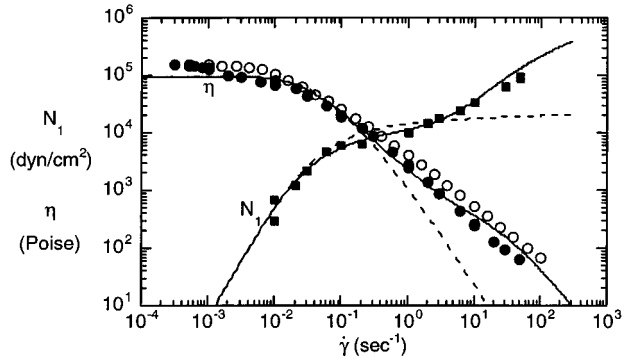

Figure 6. Comparison of the steady-state shear viscosity η and first normal stress difference N_1 predicted by the MLD (solid lines) and DEMG (broken lines) models with experimental data for polystyrene solution sample 6 (pure 8.42 M) at 40 °C. The hollow circles are for the dynamic viscosity $\eta^*(\omega)$. The model parameters are those specified in section IV.1.

the MLD and DEMG models (for simplicity, hereafter the word "toy" will be omitted). The dynamic viscosities (η^*) are also shown to test the validity of the Cox−Merz relationship, i.e., $\eta^*(\omega) = \eta(\dot{\gamma})$.[31] The models are compared with the data for monodisperse polystyrene solutions in part A., and with the bidisperse solutions in part B.

A. Monodisperse Polystyrene Solutions. Figures 5 and 6 show the comparisons of the MLD and the DEMG models with the steady-state experimental data for the monodisperse polystyrene solutions with molecular weights of 2.89×10^6 (sample 1), and 8.42×10^6 (sample 6), respectively. The dynamic viscosities (η^*) (open circles) are also shown in the figures to test the validity of the Cox−Merz relationship. For sample 1 (Figure 5), values of the dynamic viscosity $\eta^*(\omega)$ lie slightly above the steady-state shear viscosity $\eta(\dot{\gamma})$, whereas, for sample 6 (Figure 6), $\eta^*(\omega)$ is almost twice as high as $\eta(\dot{\gamma})$ at shear rates higher than 0.001. This difference indicates that the Cox−Merz relationship might be invalid for high-molecular-weight polymers. In fact, this finding is in agreement with the MLD model, which predicts the values of $\eta(\dot{\gamma})$ without Rouse stretching to be slightly lower than that of $\eta^*(\omega)$ calculated from the double reptation model (see Figure 7).

The comparison between the steady-state model predictions and the experimental data using the above-mentioned model parameters for monodisperse solutions

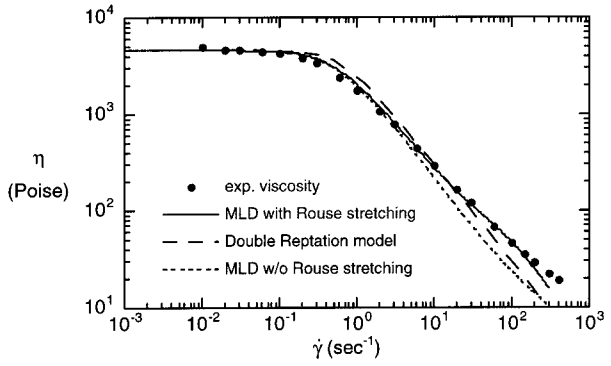

Figure 7. Predictions of the steady-state shear viscosity η by the MLD model with and without Rouse stretching and the double reptation model for sample 1. The steady-state experimental η (symbol) is also shown.

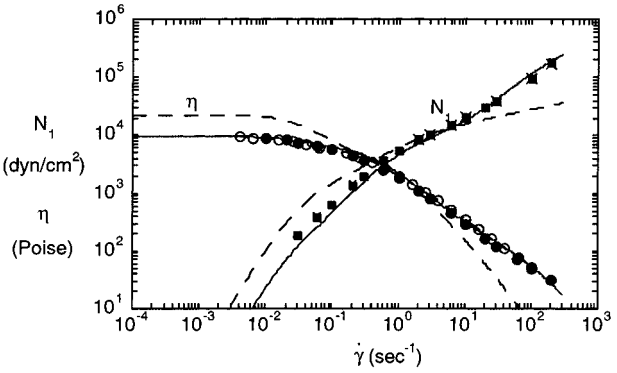

Figure 8. Comparison of the steady-state shear viscosity η and first normal stress difference N_1 predicted by the MLD (solid lines) and DEMG (broken lines) models with experimental data for polystyrene solution sample 2 (20/80 8.42 M/2.89 M) at 40 °C. The hollow circles are for the dynamic viscosity $\eta^*(\omega)$.

(Figures 5 and 6) indicates that the MLD model predictions (solid lines) are in agreement with the steady-state viscosity and first normal stress difference in both the terminal and the nonlinear regimes. The DEMG predictions (broken lines) are comparable to the MLD model at low and intermediate shear rate. At high shear rates, however, the DEMG model predicts far too much shear thinning, especially for the high-molecular-weight sample (sample 6). In fact, the DEMG model, like the original Doi−Edwards model,[3] predicts that the shear stress decreases with increasing shear rate in the strongly nonlinear regime (Figure 5), which is at odds with the experimental data.

B. Bidisperse Polystyrene Solutions. Having the model parameters fixed from part A, the predictions of the MLD and the DEMG models were obtained for the bidisperse polystyrene solutions (samples 2−5) with no additional parameters. Figures 8−11 compare the predictions of both models with the bidisperse experimental data using the same model parameters as for the monodisperse parents, discussed above. As can be seen, the reptative and convective constraint release included in the MLD model lead to much-improved predictions compared to the DEMG model even in the linear viscoelastic regime at low shear rates. In such regime, only reptative constraint release is dominant in the MLD model, thus reducing the model predictions to the double reptation formalism. On the other hand, the polydisperse DEMG model presented here reduces in the linear viscoelastic limit to the simple reptation

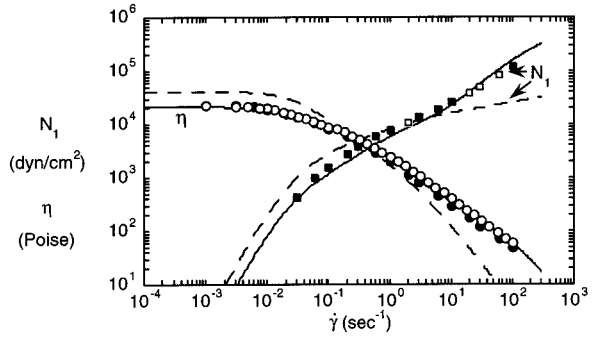

Figure 9. Same as Figure 8, except for sample 3 (40/60 8.42 M/2.89 M). The hollow squares indicate that the experimental data of N_1 barely reached steady state and the steady-state values were obtained from extrapolation.

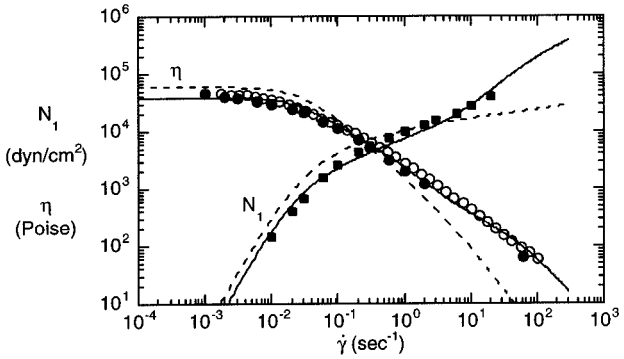

Figure 10. Same as Figure 8, except for sample 4 (60/40 8.42 M/2.89 M).

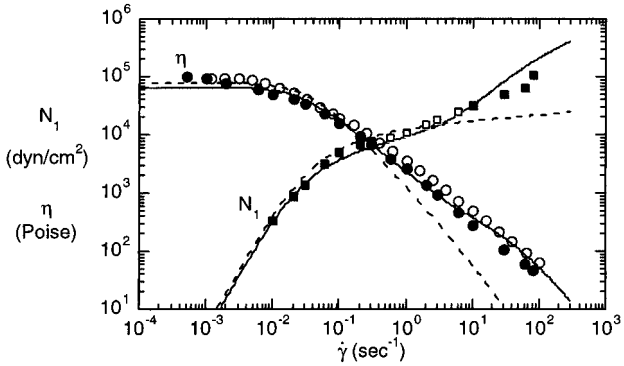

Figure 11. Same as Figure 8, except for sample 5 (80/20 8.42 M/2.89 M). The hollow squares indicate that the experimental data of N_1 barely reached steady state and the steady-state values were obtained from extrapolation.

scheme with simple linear mixing rule, which is incapable of terminal-regime predictions for bidisperse and polydisperse polymers, leading to the predictions of too high zero-shear viscosities of the blends, as well as too much shear thinning. This failure of the polydisperse DEMG model at low frequencies could easily be fixed within the DEMG theory merely by including the reptative constraint release terms.

IV.3. Predictions of Stresses in Start Up of Steady Shear. In this section, we compare the transient behavior of the shear viscosities and first normal stress differences for monodisperse solutions and the bidisperse mixtures using the same model parameters as for the steady-state predictions.

A. Monodisperse Polystyrene Solutions. In Figure 12, the transient shear viscosities $\eta(t)$ and transient first normal stress differences (N_1) predicted by the

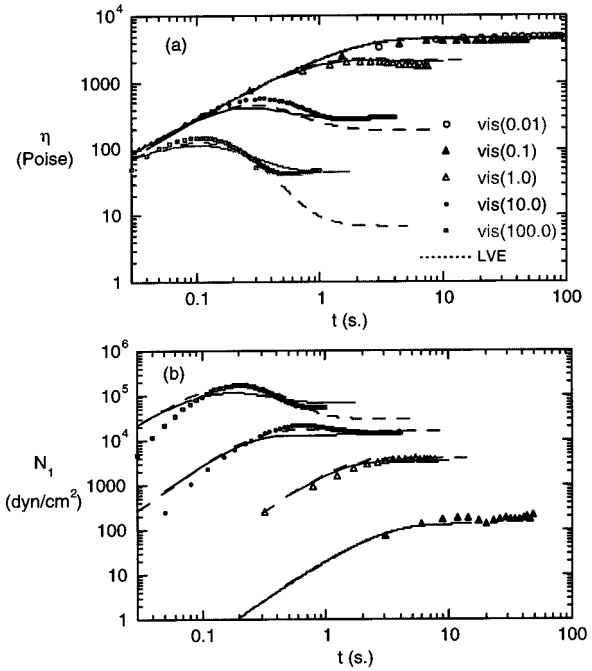

Figure 12. Comparison of the transient start up (a) shear viscosity and (b) first normal stress difference predicted by the MLD (solid lines) and DEMG (broken lines) models with experimental data for polystyrene solution sample 1 (pure 2.89 M) at 40 °C.

Table 2. Comparison of Strains at the Maximum Shear Stresses from the Experiment and from the Simplified DEMG and MLD Models

	strain at max. shear stress		
$\dot{\gamma}$	exp	DEMG	MLD
1	2.25	2.535	2.585
10	3.15	3	2.65
100	10.7	10	10.2

MLD and DEMG models are compared with experimental data in start up of shear for the monodisperse polystyrene solution with molecular weight 2.89×10^6 (sample 1). Both the MLD and the DEMG models provide good predictions at low to moderate shear rates for both $\eta(t)$ and $N_1(t)$. At high shear rates, i.e., $\dot{\gamma} \geq 10$ s^{-1}, the DEMG model predicts too much shear thinning at long times, as can also be seen from the steady-state results. At shorter times, although the shear−stress overshoots predicted by the DEMG model are in slightly better agreement with experimental data than are the predictions of the MLD theory, the peak stresses predicted by both the DEMG and the MLD models are still approximately a factor of 2 lower than the overshoots observed experimentally (Figure 12a). The strains at the maximum overshoots, however, appear to be reasonably accurate for both models as shown in Table 2. For N_1, the peak in $N_1(t)$ predicted by the DEMG model is in much better agreement with experiment than is the peak in $N_1(t)$ predicted by the MLD model (Figure 12b). At very high shear rates ($\dot{\gamma} \approx 100$ s^{-1}) after the overshoots, the observed viscosities show undershoots before the reaching steady state, which are not predicted by either model. In Figure 12, the failure in predicting the undershoots in $\eta(t)$ and $N_1(t)$ is expected for the simplified models, which neglect the dependence of orientation and stretching on the tube coordinate of the chain.[7] Note that the discrepancies between the model predictions and the experimental data at times

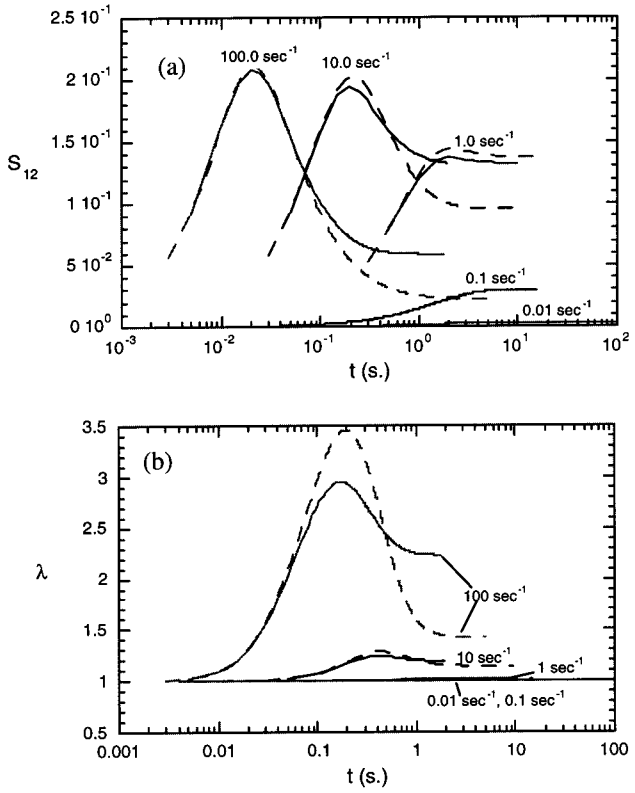

Figure 13. Comparison of (a) S_{12} and (b) λ predicted by the MLD (solid lines) and the DEMG (broken lines) models for sample 1.

shorter than 0.055 s for viscosity and 0.11 s for first normal stress difference, are artifacts from the delay in motor response and the communication from the motor to the transducer.

The contributions to shear stresses from the orientation tensor (S_{12}) and the stretch ratio (λ) predicted by the MLD model (solid lines) and the DEMG model (broken lines) are shown in Figure 13, parts a and b, for sample 1. As can be seen, the contributions from S_{12} to the overshoots in shear stress predicted by both models are similar, while the peak value of λ predicted by the DEMG model is higher than that of the MLD model at high shear rate. Since stresses are strongly dependent on λ, i.e., $\sigma \propto k_s(\lambda)\lambda^2$, the increase in λ can greatly enhance the values of stresses. The better overshoot predictions of the DEMG model, therefore, arise mainly from the larger overshoot in stretch ratio (λ). Note that the MLD model shows less maximum stretch than the DEMG model because the convective constraint release mechanism in the MLD model, though it decreases chain orientation, also reduces the stretch. The extremely low steady-state viscosity η at high shear rates predicted by the DEMG model is due to the low steady-state values of both S_{12} and λ.

Recently, Fang et al. (2000)[32] compared the molecular simulation proposed by Ottinger[33] without anisotropic cross section and the simulation by Hua and Schieber,[34−35] with the simplified version of the MLD model for the experimental data of a 13% solution of nearly monodisperse polystyrene. Although these models incorporate the same set of relaxation mechanisms (except without contour coordinate dependence for the simplified MLD model), they provide quite different predictions, especially the magnitude of the overshoots in stresses. Note that, the undershoots in stresses at

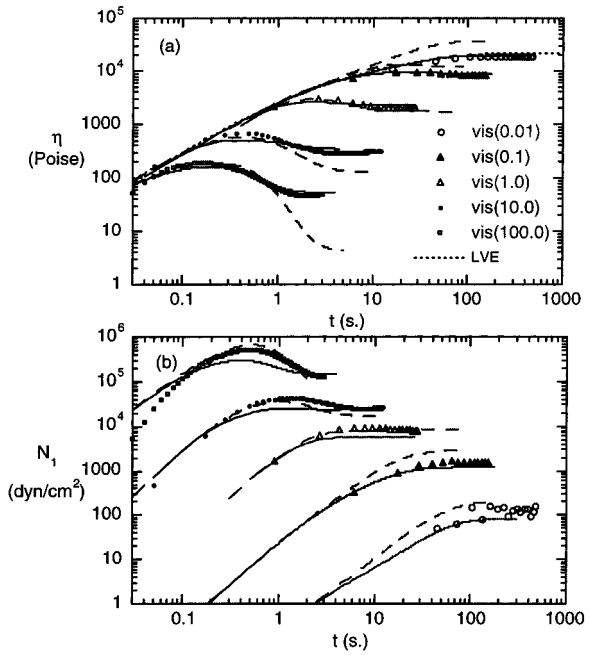

Figure 14. Comparison of the transient start up (a) shear viscosity and (b) first normal stress difference predicted by the MLD (solid lines) and DEMG (broken lines) models with experimental data for a polystyrene solution sample 3 (40/60 2.89 M/8.42 M) at 40 °C.

higher shear rates cannot be predicted from the simplified MLD model due to the neglect of the dependence of orientation and stretching on the tube coordinate. In general, the results of comparisons may depend on the polymer chosen and its number of entanglements, as well as the choice of parameters. A comprehensive comparison of the alternative models for several different well-defined samples would be worthwhile, but beyond the scope of our paper, which only looks at the MLD and the DEMG models.

B. Bidisperse Mixtures. Comparisons of the MLD and DEMG models with the binary-blend experimental data in the start up of steady shearing are shown in Figure 14 for sample 3 (PS 8.42 M/2.89 M = 40/60). The predictions of the shear viscosities and first normal stress differences of the MLD model are accurate at low and moderate shear rates. The DEMG model does not give good predictions at low shear rates, but at high shear rates, the peak values of both $\eta(t)$ and $N_1(t)$ predicted by the DEMG model are again in better agreement with the data than are the predictions of the MLD model. Similar results are also found for the start up data of the other solutions. The discrepancies between the model predictions and the experimental data at very short time ($t > 0.055$ s for η, and $t > 0.11$ s for N_1) are again due to the artifact from the finite response time of the rheometer.

The start up results indicate a possible inaccuracy of the convective-constraint-release mechanism incorporated in the MLD model. Although the CCR mechanism alleviates the extreme shear thinning for shearing flows at high shear rates, it also reduces the transient stretch rate ($\dot{\lambda}$) of the polymer chains, leading to lower predicted magnitudes of the transient stress overshoots. To improve the predictions of the MLD theory, it would appear to be necessary to reduce the effect of CCR on λ at small to modest strains, while retaining the magnitude of the effect of CCR on λ at large strain (or at long time.)

VI. Conclusions

This paper addresses the strengths and weaknesses of the simplified MLD and DEMG models for monodisperse and bidisperse entangled polymer solutions by comparing the model predictions with the experimental data for the 7% solutions of monodisperse and bidisperse high-molecular-weight polystyrenes in tricresyl phosphate. The reduced normal stresses of the solutions (relative to melts) allow data to be obtained in a conventional shear rheometer without the edge-fracture artifact. Comparison between these data and the simplified MLD and DEMG theories were made both at steady state and in start up of shearing over a wide range of shear rates. The model parameters for both theories are the disengagement time and the longest Rouse time for each monodisperse component, and the plateau modulus (G_N^0). We find that the convective-constraint-release term in the MLD model fixes the extreme shear thinning of the DEMG model at high shear rates, while the reptative-constraint-release term in the MLD model extends accurate prediction of the low-shear-rate steady-state viscosity and first normal stress difference to the bidisperse mixtures at all mixing ratios. In start up of shear, the MLD and the DEMG models are able to predict the strain at the overshoots in shear stress and in the first normal stress difference. The magnitude of the overshoots in stresses predicted by the DEMG model are in better agreement with the observed overshoots than are the predictions of the MLD model. The weakness of the DEMG model is its extreme shear thinning at high shear rate, which arises from its neglect of convective constraint release. The improvements gained in the MLD model by adding convective constraint release (CCR) and reptative constraint release via the double reptation scheme to the DEMG model does improve the steady-state predictions of the shear flows. Nevertheless, this CCR mechanism seems to decrease the transient maximum in the stretch of the polymer chains, resulting in a prediction of smaller overshoots than those of the DEMG model and of those observed experimentally. It would appear that improvement in the MLD theory might be possible if the stretch equation of the MLD model (eq 3) is changed so that the overshoot in λ is increased while the steady-state value is left nearly unchanged.

Acknowledgment. The authors are grateful to Michael K. Lyon and Michael J. Solomon for valuable suggestions on the experimental setup, and to David W. Mead, Scott D. Mishler, and Josh J. Driscoll for helping with the numerical calculations of the MLD model. C.P. is in debt to the Royal Thai Fellowship from the government of Thailand. R.G.L. is grateful for support for this work from the National Science Foundation, Grant No. DMR9807262.

References and Notes

(1) Pearson, D. S.; Kiss, A. D.; Fetters, L. J.; Doi M. *J. Rheol.* **1989**, *33*, 517.
(2) Doi, M.; Edwards S. F. *J. Chem. Soc., Faraday Trans. II* **1978**, *74*, 1789; 1802; **1818**, *1979*, *75*, 38.
(3) Marrucci, G; Grizzuti, N. *Gazz. Chim Ital*, **1988**, *118*, 179.
(4) Pearson, D.; Herbolzheimer, E.; Grizzuti, N.; Marrucci, G. *J. Polym. Sci.: Part B: Polym. Phys.* **1991**, *29*, 1589.
(5) Mead, D. W.; Leal, G. *Rheol. Acta* **1995**, *34*, 339.
(6) Mead, D. W.; Yavich, D.; Leal, G. L. *Rheol Acta* **1995**, *34*, 360−383.

(7) Mead, D. W.; Larson, R. G.; Doi, M. *Macromolecules* **1998**, *31*, 7895−7914.
(8) Marruci, G. *J. Non-Newtonian Fluid Mech.* **1996**, *62*, 279−289.
(9) Marrucci, G.; Ianniruberto, G. *Macromol. Symp.* **1997**, *117*, 223.
(10) Tsenoglou, C. *Polym. Prepr.* **1987**, *28*, 185−186.
(11) Tsenoglou, C. *Macromolecules* **1991**, *24*, 1762−1767.
(12) Cloizeaux, J. Des. *Europhys. Lett.* **1988**, *5*, 437−442.
(13) Milner, S. T. *J. Rheol.* **1996**, *40*, 303−315.
(14) Tuminello, W. H. *Polym. Eng. Sci.* **1986**, 26, 1339−1347.
(15) Mead, D. W.; Larson, R. G.; Doi. M. 2000. Private communication.
(16) Cohen, A. *Rheol. Acta* **1991**, *30*, 270.
(17) de Gennes, PG *J. Chem. Phys.* **1971**, *55*, 572−579.
(18) Fetters, L. J.; Lohse, D. J.; Richter. D.; Witten, T. A.; Zirkel, A. *Macromolecules* **1994**, *27*, 4639−4647 (the value of M_e is adjusted to be consistent with Ferry's definition.[28]
(19) Curie, P. K. *Proceedings of the Eight International Congress on Rheology*; Naples, Italy 1980.
(20) Gleissle, W. *Rheol. Acta* **1982**, *21*, 484−487.
(21) Huppler, J. D.; Macdonald, I. F.; Ashare, E.; Spriggs, T. W.; Bird, R. B. *Trans. Soc. Rheol.* **1967**, *11*, 181.
(22) Chen, I. J.; Bogue, D. C. *Trans. Soc. Rheol.* **1972**, *16*, 59.
(23) Mhetar, V. R.; Archer, L. A. *J. Polym. Sci., Part B: Polym. Phys.* **2000**, *38*, 222−233.
(24) Venerus, D. C.; Kahvand, H. *J. Polym. Sci., Polym. Phys. Ed.* **1994**, *32*, 1531−1542.
(25) Nazem, F.; Hansen, M. G. *J. Appl. Polym. Sci.* **1976**, *20*, 1355.
(26) Menezes, E. V.; Graessley, W. W. *Rheol. Acta* **1980**, *19*, 38−50.
(27) Private communication with Rheometric Inc.
(28) Ferry, J. D. *Viscoelastic Properties of Polymers*; Wiley; New York, 1980.
(29) Osaki, K.; Nishimura, Y.; Kurata, M. *Macromolecules* **1983**, *18*, 1153.
(30) Colby, R. H.; Rubinstein, M. *Macromolecules* **1990**, *23*, 2753.
(31) Cox, W. P.; Merz E. H. *J. Polym. Sci.* **1958**, *28*, 619.
(32) Feng, J.; Kröger, M.; Öttinger, H. C. *J. Rheol.* **2000**, 1293−1317.
(33) Ottinger, H. C. *J. Rheol.* **1999**, 1461−1493.
(34) Hua, C. C.; Schieber, J. D. *J. Chem. Phys.* **1998**, *109*, 10018−100027.
(35) Hua, C. C.; Schieber J. D. *J. Rheol.* **1999**, *43*, 701−717.

MA010101X